H-driven degradation of PFAS in the gas/liquid interface using electrochemistry configuration of cold plasma

A. Mota-Lima[1]

[1] *Chemical Engineering Department, Polytechnical School, University of São Paulo, Av. Prof. Lineu Prestes, 580 - Butantã, São Paulo - SP, 05508-000l, Brazil*

(Received: 27. March 2025, Accepted: 30. April 2025, Published online: 02. May 2025)

Plasma water treatment has emerged as a powerful technology capable of abate perfluoroalkyl substances (PFAS) in water matrices. With the electrochemical configuration and cathodic polarity, the electrified plasma/liquid interface (EPLI) not only produces in-situ hydrated electrons (e_{aq}^-) that readily react with PFAS, but also produced radicals in the plasma effluent. This study uses chemical reaction networks (CRN) to investigate the chemical pathways of PFAS degradation by EPLI-induced e_{aq}^-, allowing for a direct comparison with the bench experiments of Stratton et al. (Environ. Sci. Technol. 2017, 51, 3, 1643) and Alam et al. (Chemical Engineering Journal, 2024, 489, 151349) degrading PFOA (Perfluorooctanoic Acid) and PFOS (Perfluorooctane Sulfonate), respectively. The computational results indicate that Perfluorooctanoic Acid (PFOA) degradation by EPLI-induced e_{aq}^- has a Faradaic efficiency of less than 0.01% given the typically low concentration of PFOA in water matrices, meaning that the majority of e_{aq}^- engages with water reduction, generating gaseous hydrogen. EPLI-induced e_{aq}^- alone cannot account for the energy efficiency observed in bench experiment of Stratton et al. and Alam et al., suggesting the presence of other plasma-induced radicals. This work evaluates the gas-phase H radical as crucial for degrading PFOA at the gas/liquid interface, which is created by the plasma effluent in contact with the water matrix. This work paves the way for construct effective plasma-based industrial reactors to degrade PFAS, suggesting the formation of radical-H in the plasma effluent as a key parameter to be optimized.

(DOI: 10.31281/vab52w73)

mota@usp.br

I. Introduction

Plasma electrochemistry creates the electrified plasma/liquid interface (EPLI) known for simultaneous production of hydrated electrons (e_{aq}^-) in the aqueous phase, [1] along with the co-production of both hydrogen peroxide (H_2O_2) [2-5] and hydrogen (H2) [5, 6] in the gaseous effluent of the plasma phase. This phase separation, regarding the in-situ production of both e_{aq}^- and H_2O_2 via plasma electrochemistry, offers an unprecedented approach to building innovative reactors for the mineralization of emerging micropollutants. However, the use of EPLI-induced e_{aq}^- for environmental remediation remains largely unexplored, except for the work of Thagard & Holsen, [7-10] who extensively employed the electrochemical configuration of cold plasma to degrade recalcitrant pollutants like per- and polyfluoroalkyl substances (PFAS).

In this work, chemical reaction networks (CRN) are proposed to explain the degradation of PFAS both by EPLI-induced hydrated electrons (e_{aq}^-) and by other plasma-induced gas phase radicals at the gas/liquid interface. Two PFAS are elected in this work, namely Perfluorooctane Sulfonate (PFOS) and Perfluorooctanoic Acid (PFOA). According to ab-initio calculations, all carbon center in PFOA molecules has similar susceptibility to cleavage the C-F bond after the

hydrated electron interaction, being all the computed free energy barriers relatively low, [11] which in turn manifests in a macroscopic hierarch as an elevate rate constant for the reaction between e_{aq}^- and PFOA. In agreement to that, the rate constant of 108 and 109 L mol−1 s−1 were measured using bench experiments [12] for the reaction between e_{aq}^- and pollutant, either PFOA ($C_8HF_{15}O_2$) or PFOS ($C_8HF_{17}O_3S$) respectively.

$$e_{aq}^- + C_8HF_{15}O_2 \xrightarrow{k1} radical^\bullet + F^- \quad (1)$$

$$e_{aq}^- + C_8HF_{17}O_3S \xrightarrow{k2} radical^\bullet + F^- \quad (2)$$

Fig. 1 depicts the EPLI generated during plasma electrochemistry, where a metallic tip (first electrode) and a counter metallic plate (second electrode) work together to confine a high electric field within a narrow volume, within which cold plasma evolves, as highlighted in red. Compared to conventional electrochemistry, plasma electrochemistry presents several distinct characteristics, as outlined below. In the plasma electrochemistry, there are two configurations for the working electrode: contacting and contactless solid electrode. [13] The liquid must be conductive for direct-current (DC) operation; however, if the electrolyte is non-conductive, such as ultrapure water, alternating current (AC) must be used exclusively. The second electrode (or counter electrode) can also be configured as either the contact or contactless, but if a dielectric material, such glass, is placed between the metallic electrode and the liquid, only alternating current is permitted.

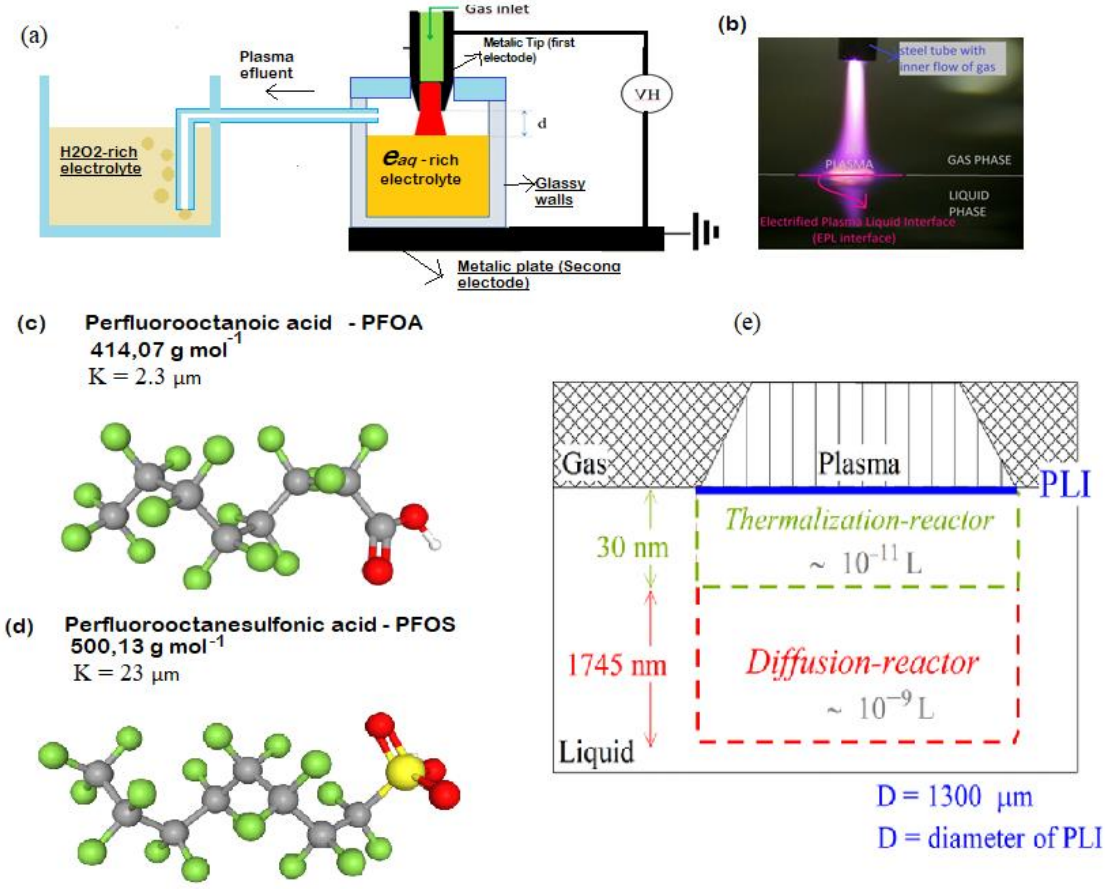

Figure 1: (a) sketch of the electrified Plasma-liquid interface (EPLI) reactor, highlighting the hydrated electron generated beneath the EPLI and the co-generation of H_2O_2 in a second vessel as observed by Rumbach et al.,[2] and, chemical Structure of (b) Perfluorooctanoic acid –PFOA– (c) and Perfluorooctanoic acid – PFOS. (d) photograph of a jet cold plasma observed at Hokkaido University by Prof. Naoki Shirai. (e) Sketch of the reaction zone showcasing thermalization penetration of e_{aq}^-, which defines the volume of the thermalization reactor, and a diffusion length of e_{aq}^-, which defines the volume of the diffusion reactor; reprinted with permission from "J. Phys. Chem. C 2020, 124, 20, 10907–10915." Others: HV = high voltage; d = distance between the metallic-tube tip and the water surface (electrolyte surface); red = plasma jet; Black = metallic part; blue = glass; green = gas flow; yellow= water enriched with peroxydisulfate ion. Letter K stands for the adsorption coefficient at the gas/liquid interface for each pollutant, [15] and relates to the ratio surface excess to bulk concentration of such pollutant.

Fig. 1a shows both the working and counter electrodes in a contactless configuration, and given the presence of a glass layer between the counter electrode and the liquid, only alternating current is allowed for the electrochemical cell in this figure. Fig. 1b presents an image of jet plasma focusing on the electrified plasma/liquid interface. When negative plasma polarity is used, EPLI produces solvated electrons in the water matrix, [1] as shown in Fig. 1a, while all the $H_2O_2$is produced in the humidified gas where the plasma/discharge develops. It is possible to collect the H_2O_2 in a second vessel [2] after scrubbing the plasma effluent in water. Since e_{aq}^- and H_2O_2, are produced in liquid and gas phase, respectively, they are generated in two spatially different reactors. In the electrochemical configuration, two open reactors are created. The plasma functions as an open reactor where molecules of water vapour are broken down to generate radicals, [6] which in turn, participates in reaction that leads to stable final products such as gaseous H_2 [6] and H_2O_2 [2].The second open reactor encompasses the liquid phase beneath the EPLI, as drawn in Fig. 1e. Such an electrochemical reactor is sketched in Fig. 1e, which shows the thermalization reactor where a ballistic electron undergoes solvation and losses its kinetic energy, while the diffusion reactor depicts hydrated electrons (e_{aq}^-) diffusing in the bulk liquid [14].

The earliest plasma reactors for environmental remediation employed the torch-like gas-phase discharge configuration, which involve ordinary plasma liquid interface. The torch configuration utilizes the plasma phase as the reactor to produce radicals and oxidative species like ozone (O_3) and hydrogen peroxide (H_2O_2). Such torch-like configuration demonstrated effective to destroy gas-phase pollutant (volatile organic compounds) such as toluene [16] and ethylene, [17] as well as PFAS like hexafluoroethane [18]. If instead the pollutant is in liquid phase, the plasma-phase radicals need to be brought into contact with aqueous pollutant using a variant configuration. Two variant configurations of ordinary plasma liquid interface have been deployed to abate PFAS. In the reactor developed by Johnson et al., the original plasma/gas interface (or plasma edge) is replaced by the ordinary plasma liquid interface using an annular flow, [19] i.e. this type of flow is characterized by the presence of a liquid ring moving around a gas or vapor nucleus. The second variant involves the bubbling of the plasma effluent directly into the water matrix [20]. On the other hand, the research group led by Thagard and Holsen [7-10] at Clarkson University, along with recent studies from the University of Sydney, [21, 22] has been at the forefront of environmental remediation of PFAS using a truly effective EPLI. Their studies have shown that EPLI can be successfully employed to degrade PFAS in water matrix. Allam et al. [21, 22] demonstrated that the bubbling of gas in the bottom of the reactor promotes a convective mass transfer of PFAS from the bulk bottom to the top surface. Ultimately, this finding allows us to infer that gas/liquid interface (not only electrified EPLI) is the spatial location were significant PFAS degradation occurs. This work addresses the mechanisms by which each reductive species is produced at different interfaces induced by cold plasma. This study presents the dynamical analysis of the stoichiometric chemical reaction networks (CRN), proposing mechanisms for the reactivity of hydrated electron and radicals in the context of PFAS degradation. Our investigation aims to establish a deeper understanding of the PFOA/PFOS degradation mechanism, providing a reasonable explanation for the remarkable degradation performance observed in the work of Thagard & Holsen and Adam et al.

II. Theory

II.a) Intrinsic reaction of the hydrated electron e_{aq}^- and Radicals in water matrix

The solvated electron (e_{aq}^-) induced by the plasma electrochemistry (cathodic discharge over water) engages with the water oxidation, leading to the hydrogen production [23].

$$2e_{aq}^- + H_2O \xrightarrow{k3} H_2 + 2OH^- \quad (3)$$

The hydronium ions provide an additional route for H_2 production [24]

$$e_{aq}^- + H_{aq}^+ \xrightarrow{k4} H^\bullet{}_{aq} \quad (4)$$

$$e_{aq}^- + H^\bullet{}_{aq} + H_2O \xrightarrow{k5} H_2 + OH^- \quad (5)$$

$$2H^\bullet{}_{aq} \xrightarrow{k6} H_2 \quad (6)$$

Finally, the reaction between intermediate and reactant of the CRN-3

$$H^\bullet{}_{aq} + C_8HF_{15}O_2 \xrightarrow{k7} radical^\bullet + F^- \quad (7)$$

II.b) Plasma-electrochemistry Reactor

Fig. 1e outlines the EPLI, emphasizing the spatial position of the reactor termed EPLI-reactor

located right beneath the EPLI. The EPLI is an open reactor containing a volume of 10^{-9} L or even 10^{-12} L because it depends mainly on the geometry of the plasma-liquid contact [25]. A detailed estimation on the volume EPLI reactor ponders the time scales for both the chemical and the diffusional events related to the local concentration of hydrated electrons (e_{aq}^{-}) [24].

II.c) CRN-1 and CRN-2 mathematical model

The PFOA and PFOS minimum mechanism of degradation induced hydrated electrons in the EPLI is seen in Fig. 2. The set of ODEs describing the free-variables of the CRN-1 and CRN-2 gathers Eqs. from (8) to (11).

$$\frac{d[e]}{dt} = \frac{q_e}{V} - [e]\{k_1[\mathrm{P}] + 2\,k_3[e] + k_4[H^+] + k_5[\mathrm{H}\bullet]\} \quad (8)$$

$$\frac{d[\mathrm{P}]}{dt} = [\mathrm{P}]_0 - k_1[e][P] \quad (9)$$

$$\frac{d[\mathrm{H}^+]}{dt} = [\mathrm{H}^+]_0 - k_4[\mathrm{e}][\mathrm{H}^+] \quad (10)$$

$$\frac{d[\mathrm{H}\bullet]}{dt} = k_4[\mathrm{e}][\mathrm{H}^+] - \{k_5[e][\mathrm{H}\bullet] + 2k_6[\mathrm{H}\bullet]^2\} \quad (11)$$

Either CRN-1 or CRN-2 form a linear system of ODEs containing four free-variables, namely $[e]$, [P], [H•] and [H+], which stands for the local concentration of hydrated electrons, pollutant, radical hydronium, and hydrogen ion, respectively. The time evolution of those four free-variable can be seen in Fig. 3, and the parameters used in the numerical solution of the linear system of ODEs listed in Tab. 1. The variable [P] was replaced by [PFOA] for CNR-1, meaning the local concertation of PFOA. The same applies for CNR-2, to which [PFOS] replaces [P], meaning the local concertation of PFOS. Furthermore, the initial concentration of pollutant in the ODE system, that is represented by the parameter $[P]_0$, was replaced by $[PFOA]_0$ and $[PFOS]_0$ respectively for CRN-1 and CRN-2. And finally, when dealing with CRN-2, it was used values of $k_2$instead of k_1 everywhere in the set of Eqs. (8) to (10).

II.d) CRN-3 mathematical model

The set of ODEs describing the free-variables of CRN-3 gathers Eqs. from (12) to (15).

$$\frac{d[e]}{dt} = \frac{q_e}{V} - [e]\{k_1[\mathrm{PFOA}] + 2\,k_3[e] + k_4[H^+] + + k_5[\mathrm{H}\bullet]\} \quad (12)$$

$$\frac{d[\mathrm{PFOA}]}{dt} = -\{k_1[e][PFOA] + k_7[\mathrm{H}\bullet][PFOA]\} \quad (13)$$

$$\frac{d[\mathrm{H}^+]}{dt} = -k_4[\mathrm{e}][\mathrm{H}^+] \quad (14)$$

$$\frac{d[\mathrm{H}\bullet]}{dt} = k_4[\mathrm{e}][\mathrm{H}^+] - \{k_6[e][\mathrm{H}\bullet] + 2k_6[\mathrm{H}\bullet]^2 + + k_7[\mathrm{H}\bullet][PFOA]\} \quad (15)$$

Parameters	Values	Unit	Ref.	meaning
k_1	1.0×10^8	L mol^{-1} s^{-1}	[12]	Rate constant of reaction 1
k_2	1.0×10^9	L mol^{-1} s^{-1}	[12]	Rate constant of reaction 2
k_3	6.0×10^9	L mol^{-1} s^{-1}	13	Rate constant of reaction 3
k_4	2.3×10^{10}	L mol^{-1} s^{-1}	13	Rate constant of reaction 4
k_5	2.5×10^{10}	L mol^{-1} s^{-1}	12	Rate constant of reaction 5
k_6	1.0×10^{10}	L mol^{-1} s^{-1}	12	Rate constant of reaction 6
k_7	4.0×10^7	L mol^{-1} s^{-1}	12	Rate constant of reaction 7
q_e (8 mA) (Sankaran)	82.91×10^{-9}	mol s^{-1}	[2]	Rate of electron injection @ 8 mA
$[e]_0$	zero	mol L^{-1}		Initial concentration of hydrated electron
$[PFOA]_0$	2.0×10^{-5}	mol L^{-1}		Initial concentration of PFOA
$[PFOS]_0$	2.0×10^{-5}	mol L^{-1}		Initial concentration of PFOS
$[H^+]_0$	$10^{-5.9}$	mol L^{-1}	11	Initial concentration of hydrogen cation
$[H^{\bullet}]_0$	zero	mol L^{-1}		Initial concentration of hydrogen Radical
V (Gonzalez)	2.36×10^{-9}	Liter	11	Volume of the reactor beneath the EPLI

Table 1: Parameters of the CRN used in the computational experiments.

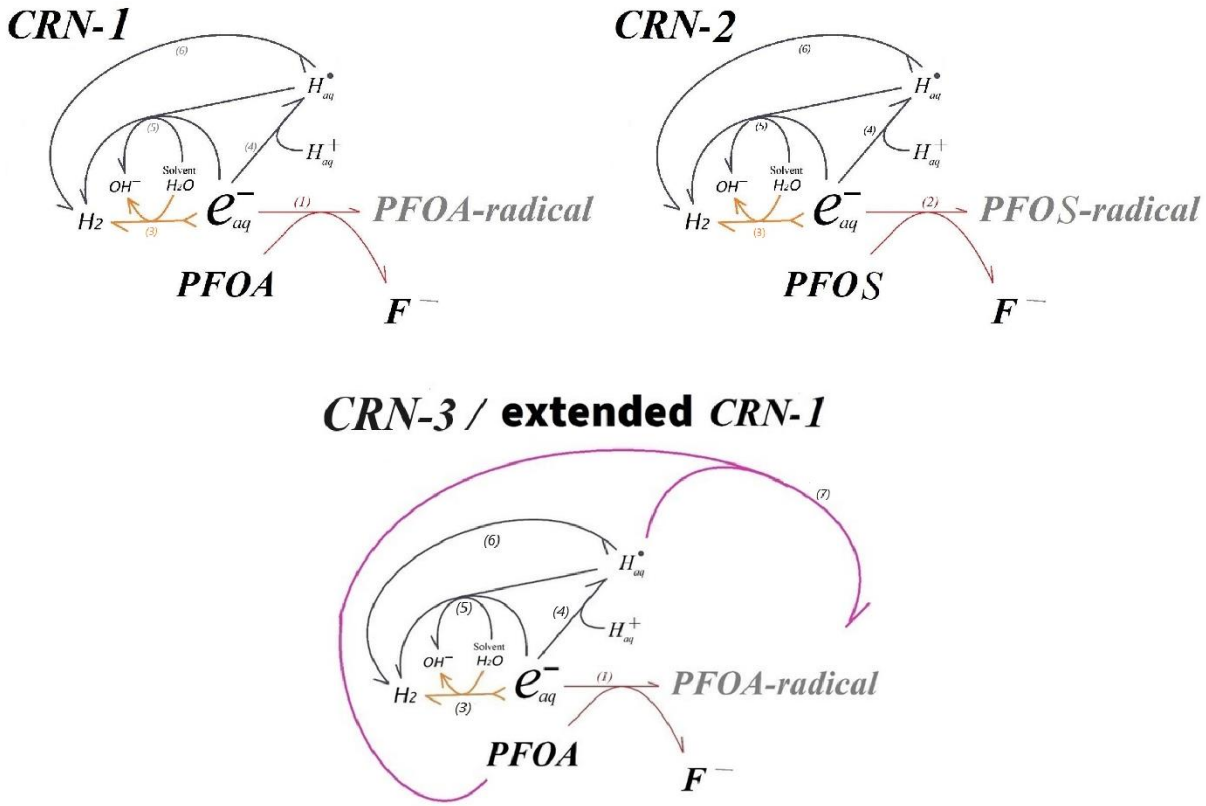

Figure 2: Chemical reaction networks (CRNs) for the core mechanism of hydrated electron interaction respectively with PFOA and PFOS, named CRN-1 and CRN-2, as well as CNR-3 that includes the reaction between PFOA and aqueous radical H.

Where the free-variables $[e]$, $[\mathrm{PFOA}]$, [H•] and [H+], stands for the local concentration of hydrated electrons, PFOA, radical hydronium, and hydrogen ion, respectively.

II.e) Computational method

To access the temporal evolution of the independent variables, the linear system of ordinary differential equations was solved via interactive method carried out with Wolfram language (Wolfram Mathematica). The Wolfram command NDSolve was used to solve the linear system of ordinary differential equations. The full Wolfram code used to solve CRN-1 is found in section C of the material supporting.

II.f) Electrical variables of Plasma

As this work aims to connect the kinetics of PFOA degradation with the energy performance of the water treatment, our simulations use electrical variables observed in the lab of prof Mohan Sankaran [2], i.e., DC micro-plasma with 8 mA and 470 V, to which 3.76 W is estimated, cf. Tab. S1 in the supporting material. The power density (PD) is estimated in Tab. S2.

II.g) Faradaic Efficiency

In a mechanism like CRN-1, there are three final products, namely H_2, PFOA-radical and ion F^-. Basically, the mathematical definition for Faradaic efficiency (FE) is

$$FE = n_i \frac{\#p_i}{\#e} \tag{16}$$

Where for a given pathway $\#p_i$ means the number of moles of a given product i, n_i is ratio the stoichiometric coefficient of the electrons to the stoichiometric coefficient of the product p_i, and #e means the total number of moles of electrons effectively crossing the plasma/liquid interface. For negatively biased plasma (cathodic plasma), the total number of ballistic electrons from the plasma that effectively crossed the EPLI is regarded as hydrated electrons. In an electrified plasma/liquid interface (EPLI) such

number is well defined because, in principle, a closed electrical circuit has the same current (j) at any point of the circuit. Thus, the electrical current measured at any point in the external circuit must be quantitatively equal to the current crossing the EPLI. The same approach is not applied to an ordinary plasma/liquid interface, making experiments with EPLI particularly convenient for studying chemical mechanisms. The total number of electros is related to the external current (j) by

$$\#e = \frac{jt}{F} \quad (17)$$

Where t is time of the measurement, and F is the Faraday constant.

Faradaic efficiency (FE) informs the percentage from the total number of electrons drained towards synthesis of a specific final product. In the mechanism described in CRN-1, the route of hydrogen production has three pathways, namely reaction (3), reactions (4) + (5), and reaction (4) + (6); all these pathways have $n_{H2} = 2$ afer considering the balance global reaction. On the other hand, the products PFOA-radical and ion F^- have $n_{F^-} = n_{\mathrm{PFOA-radical}} = 1$.

III. Results and Discussion

III.a) CRN-1, CRN-2 and CRN-3 analysis for the electrified plasma liquid interface (EPLI)

Fig. 3 shows the degradation decay of PFOA (plate a) and PFOS (plate c), both at initial concentration of 20 μM, when ultrapure water is submitted to 8 mA of Argon based jet-plasma discharge. The abatement of 90 % of such initial concentration hits faster time span for PFOS, ca. 1.96 ms, than for PFOA, ca. 7,51 ms, which merely reflects the higher rate constant of hydrated electrons scavenger by PFOS than by PFAS ($k_2 = 10k_1$). Second important aspect of the dynamics exhibits by the EPLI-induced PFOA/PFAS degradation relates to the local concentration of solvated electrons, which is notoriously high at t_{90} (time it takes to abate 90 % of initial pollutant concentration), firing the velocity of the reactions related to the hydrogen synthesis in water phase.

The extension of the hydrogen synthesis along the t_{90} span can be evaluated by computational experiments considering the time evolution of hydrogen concentration is a dependent-variable of CRN-1, thus it can be expressed by

$$\frac{\mathrm{d[H_2]}}{\mathrm{dt}} = \mathrm{k_4[e]^2 + k_6[e][H\bullet] + k_7[H^+]} \quad (18)$$

And the mole production of hydrogen can be obtained by first coupling the Eq. 18 to the time evolution of local concentration of [e], [H^+] and [H•], second dividing the Eq. 18 by the EPLI-reactor volume, and third integrating the resulted Eq. 18 over time. Fig. 4a shows the results after considering this procedure for CRN-1. For comparison, the time evolution of EPLI-crossing electrons for current of 8 mA is also shown, and it follows a linear equation whose coefficient value is displayed in Tab. 1 for qe (8 mA). The calculation of Faradaic efficiency (FE) is given in percentage in Fig. 4b. Calculated FE for H_2 synthesis is of 72 % ($442.72 \times 10^{-12} \div 622.65 \times 10^{-12}$). In Fig. 4b, the moles of EPLI crossing electrons (e-plasma) along with the moles of electrons related to the products (either H2 or PFOA radical) were obtained for the time of 7.51 ms, which is the t_{90} found in Fig. 3a. The number of electrons drained toward H_2 synthesis was found by multiplying by two the amount of hydrogen found in Fig. 4a ($2 \times [221.36 \times 10^{-12}]$), because this is the stoichiometry of Eq. 3. The same stoichiometry is valid for other routes of H_2 production [24].

Fig. 4b demonstrates that the gaseous hydrogen is the major final product of an EPLI-based water treatment. Over 72 % of all in-situ hydrated electrons generated by EPLI is drained toward hydrogen production in liquid phase, and the PFOA-radical is the minor final product, consuming less than 0.01% of all EPLI-generated hydrated electrons.

Tab. 2 compares the overall performance of the empirical theoretical results of this work with bench experiments. Among the bench experiments reporting PFOA degradation it was found that of Stratton et al. [8] employing pulsed plasma in an Argon-jet EPLI and that of Hayashi et al. [20] using DC plasma in a torch-like Oxygen-jet. Both the initial PFOA concentration, power density (PD = input power/treated volume) and the apparent first-order rate constant (k_{obs}) observed in these works (k_{obs}) were collect in Tab. 2. The t_{90} span (t_{90} = 1/ k_{obs}) and overall energy performance (= t_{90}^{-1} / PD, energy per order of PFOA decay) was calculated for these bench works. Compared to the performance of the CRN-1, both bench works lead to much better energy performance. One thousand better energy performance for the work of Stratton et al., and around four times better energy performance for the work of Hayashi et al.

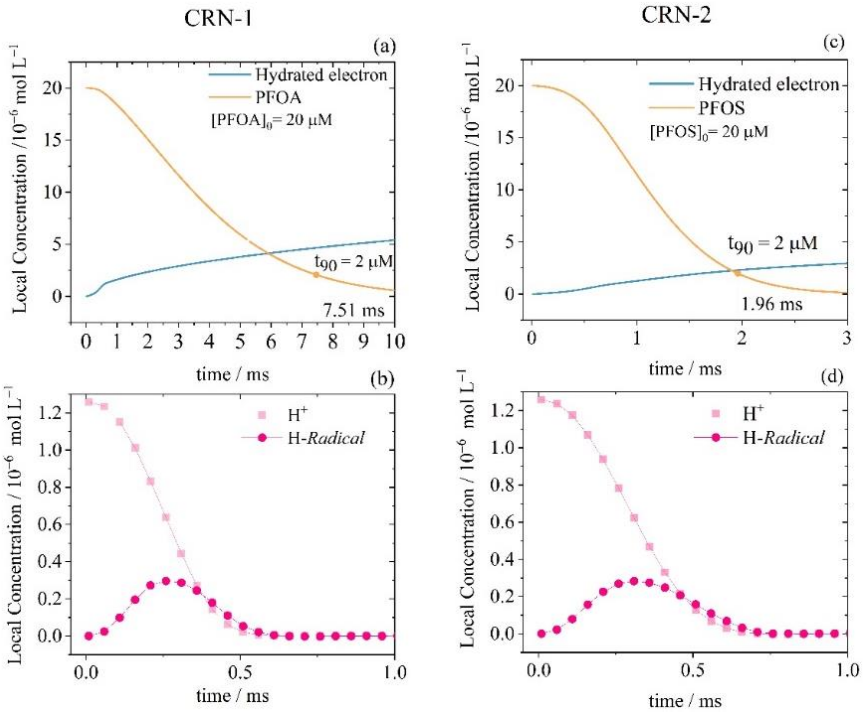

Figure 3: Local concentration of (a,c) hydrated electron plus PFOA/PFOS in a large time scale, and of (b,d) hydrogen ion and hydrogen radical in a short time scale. Numerical solution of CRN-1 (first column) and CNR-2 (second column) was obtained with computational experiments using parameters from Tab. 1 for current of 8 mA, pH of 5.9, and local reactor volume of 2.36 nL.

Treatment	$[PFAS]_0$ μM	Electrical Properties	k_{obs} (min^{-1})	t_{90} (min)	PD (W/L)	$\frac{t_{90}^{-1}}{PD}\left(\frac{min^{-1}}{W\,L^{-1}}\right)$	Ref.
Pulsed plasma in Ar	20	Pulsed, High rate	0.074	13.51	54.6	13.55×10^{-4}	[8]
Pulsed plasma in Ar	20	Pulsed, High efficiency	0.012	83.33	2.9	41.29×10^{-4}	[8]
DC plasma in O_2	100	DC	0.030	33.33	1550	0.19×10^{-4}	[20]
DC plasma in Ar, 2.36 nL	20	DC, 8 mA **	—	12.51×10^{-5} (7.51 ms)	1.59×10^{9}	0.05×10^{-4}	CRN-1, This work
DC plasma in Ar, 2.36 nL	20	DC, 8 mA	—	5.20×10^{-5} (3.12 ms)	1.59×10^{9}	0.12×10^{-4}	CRN-3, This work
Pulsed plasma in Ar, and Medium Bubble	0.27	Pulsed	0.014	73	40.0 *	3.50×10^{-4}	[21]
Pulsed plasma in Ar and Fine Bubble	0.27	Pulsed	0.095	10.5	40.0 *	23.75×10^{-4}	[21]
Pulsed plasma in Ar	20	DC, 8 mA	—	3.26×10^{-5} (1.96 ms)	1.59×10^{9}	0.19×10^{-4}	CRN-2, This work

* For the reference 21, the volume of the reactor was considered as 12.5 L (25L divided by 4), and electrical energy for t90 of 0.25 kW.

** It was used DC plasma (or constant current) observed in reference [6] J.R. Toth, R. Hawtof, D. Matthiesen, J.N. Renner, R.M. Sankaran, On the Non-Faradaic Hydrogen Gas Evolution from Electrolytic Reactions at the Interface of a Cathodic Atmospheric-Pressure Microplasma and Liquid Water Surface, Journal of The Electrochemical Society 167(11) (2020) 116504.

Table 2: Performance indicator of this work in comparison to bench experiments using EPLI configuration to degrade PFAS, except by reference [20] that uses an ordinary Plasma liquid interface.

The energy performance mismatch between our CNR-1 analysis and the bench experiments from Stratton et al. [8] can be rationalised as follows. Our generalist hypothesis is that the CRN-1 oversimplifies the EPLI-induced PFOA mechanism of degradation because it considers none interaction between PFOA and in-situ readily formed radicals. A close look on the CRN-1 demonstrates the formation of radical H as result of reaction 4. The interaction between PFOA and such hydrated-electron induced radical H is considered in the extended CRN–1, which passed to be named CRN-3 henceforth. To advance in this front, we carried out computational experiments with an extended CRN–3, shown in Fig. 2, being the major results shown in Fig. S1 of the Supporting material. It was found that pH below 3 decreases t_{90} the most. Values of t_{90} tends to 3.12 ms for CRN–3 against 7.51 for CRN–1. Yet, no better energy performance for extend CRN–1 justify the experimental findings of Stratton et al. As shows Tab. 2, energy performance of 0.12×10^{-4} L min^{-1} W^{-1} for extend CRN–1 against 13.55×10^{-4} L min^{-1} W^{-1} for bench experiments of Stratton et al.

Discharge in pure oxygen is known to generate O atoms in plasma phase, rendering ozone (O_3) in gas phase.[27] The plasma reactor in the work of Hayashi et al. follows an ordinary plasma liquid interface where the plasma effluent is brought into contact with the liquid phase by bubbling the plasma effluent into the water matrix. We can safely argue that readily formed O_3 passes to oxidize the PFOA in the ordinary plasma effluent/liquid interface. In principle, the number of e_{aq}^- formed in this interface is mild, if not negligible, in comparison to the EPLI. It is likely that O_3 is the underlying specie degrading PFOA in the bench experiments of Hayashi et al. Presumably, the slight better energy performance of O_3 toward PFOA degradation ($5 \times 10^{-4}\, min^{-1}/W\, L^{-1}$) in comparison to that of CNR-1 ($19 \times 10^{-4}\, min^{-1}/W\, L^{-1}$) has to do with the amount of O_3 formed in the plasma-phase.

On the other hand, the bench experiments of Stratton et al. do deal with an EPLI experiment and, yet, there is not a direct explanation to justify such 1000x better energy performance in comparison to that of CRN-1, if not considering the extra source of radicals along the discharge itself. We suspect that the extra radicals have origin outside the EPLI reactor. Such unaccounted radical would abate part of the PFOA, resulting in a larger PFOA decay than expected for our CRN-1. The argon-jet discharge is known to promote water splitting via electron impact when water vapour is present in noble-gas discharge, [6] which is an experimental condition quite similar to that used by Stratton et al. Among the water fragments formed this way is the H atom, which is a long-living species in Argon gas, being the reason for H atoms survive long enough in Argon until react out with PFOA in the plasma effluent/liquid interface. Such effect seems to be intensified in the experiments of Stratton et al. due to the recirculation of the plasma effluent from the headspace of the reactor by bubbling it directly into the water matrix, which increases the geometric area between plasma effluent and liquid. Additionally, the gaseous hydrogen produced by the CRN-1, as demonstrated with the results of Fig. 4, can be readily converted into H atom when it escapes EPLI-reactor toward the headspace where the discharge develops.

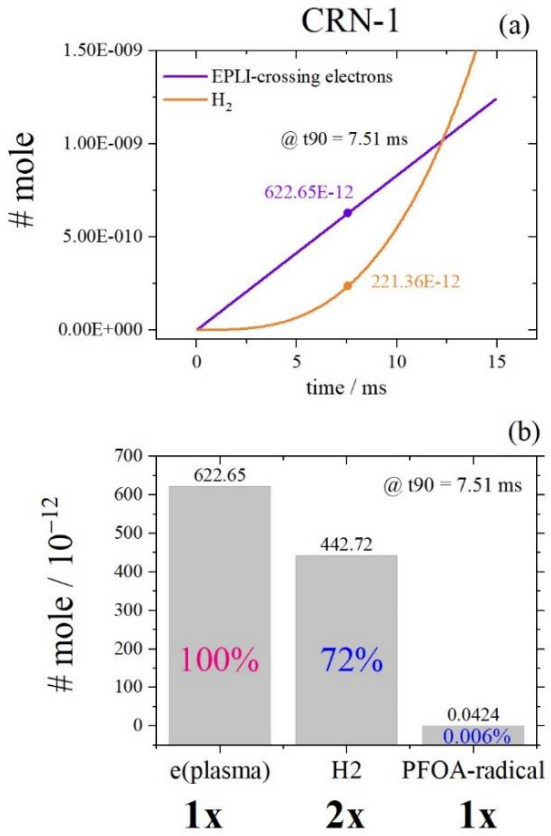

Figure 4: (a) number of moles of gaseous hydrogen produced by CRN-1 (cf. Eq. 16) along with the number of moles of ballistic electrons injected from plasma into the liquid, which is represented by the term q_e (8 mA) in Tab. 1; (b) moles of injected electrons compared to the products at the time of 7.51 ms. Faradaic Efficiency is shown in percentage. Parameters set employed in the numerical solution are the same used in Fig. 3.

Very presumably, both sources of H atom are the unaccounted origin of species acting as extra

radicals in the bench experiments of Stratton et al. Finally, other plasma species like OH and O are also formed during the electro-impact induced water split in the plasma phase, but the former readily forms H_2O_2 and the latter is negligibly in total number. Alone, H_2O_2 could not justify the PFOA abatement.

III.b) Polarity of Plasma used by Stratton et al. and by Alam et al.

The polarity of plasma has a profound impact on the nature and quantity of specie created beneath EPLI (EPLI reactor). Cathodic plasma generates hydrated electron in the EPLI reactor,[1] with a ratio of one hydrated electron to one electron from the external circuit. In the cathodic plasma, the plasma is negatively biased while the water surface is positively biased (or water anode). If instead, the polarity is inverted, being the plasma positively biased (or plasma anode) while the water surface being negatively biased (or water cathode), we have the anodic plasma that generates H_2O_2 in the EPLI. [28, 29] Recently, Researchers from Notre Dame University found that anode plasma generates aqueous radical OH in the EPLI, [30] which in our interpretation is an intermediate specie that gets recombined to form H_2O_2. The same authors also noted FE of half hydrated electron and twice aqueous radical OH per one electron from the external circuit.[30] Our only reservation about this work is that the authors showed an negatively biased plasma polarity, which, in principle, is an cathodic plasma and not a anodic plasma as intended by the authors. From that, it is evident our criticism about the interfacial polarity when employing the electrochemical configuration of cold plasma. The importance of both the polarity and waveform of the plasma electrical properties to the local production of hydrated electrons are highlighted here. Fig. 5 shows the waveform of either current or potential of the plasma observed by Stratton et al. and by Adam et al. The experiments at Clarkson University evolves with a mix of positive and negatively biased plasma potential. More importantly, the negatively biased potential hits -5kV against approximately +15kV for the section of positively biased potential. On the contrary, the experiments at Sidney University displays only positively biased potentials of plasma, meaning that experiments of Alam et al is very less specialized in producing hydrated electrons than the experiments of Stratton et al. Yet, the energy performance observed in both the universities are commensurable, cf. Tab. 2 that shows performance between 3.25×10^{-4} and 23.75×10^{-4} L min^{-1} W^{-1} for experiments of Alam et al. and between 13.55×10^{-4} and 41.29×10^{-4} L min^{-1} W^{-1} for experiments of Stratton et al.

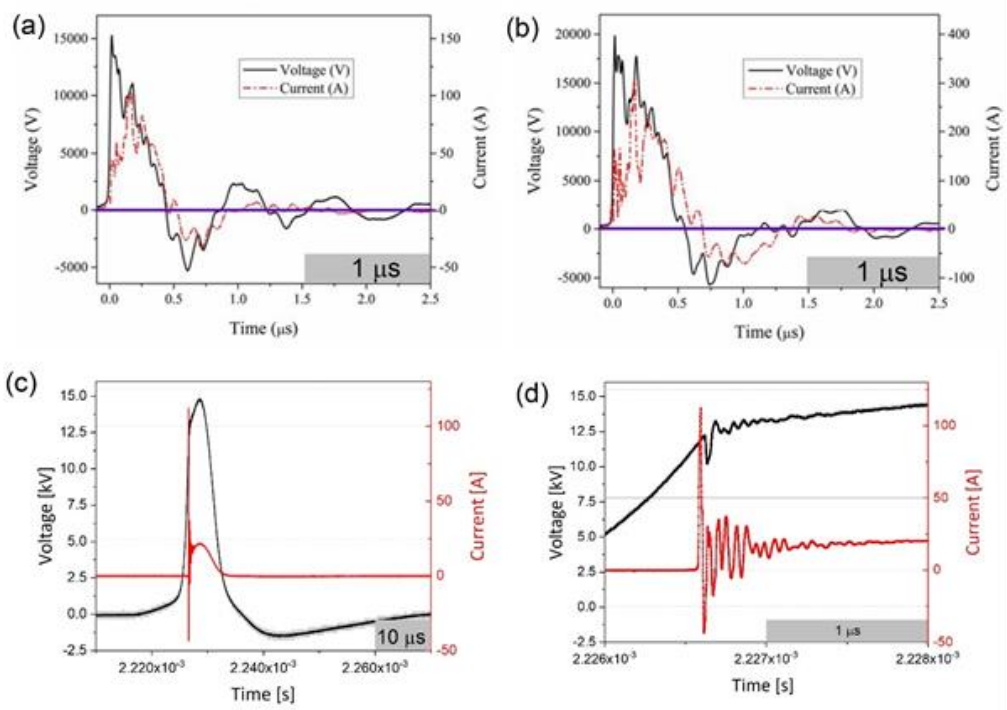

Figure 5: Current and potential time evolution of the cold plasma in the electrochemical configuration employed by the Stratton et al. at Clarkson University (a) for the high efficiency and (b) high-rate experiments, [8] as well as that employed (c) by Alam et al. at Sidney University including (d) a zooming in the region of electrical instability.[21] Figures adapted with permission.

While the plasma polarity is crucial for the generation of hydrated electrons within the EPLI reactor, it has none impact on the spectrum and quantity of radicals formed in the plasma and plasma effluent. The density of free electrons in plasma is one of the key parameters determining quantity of radicals in the plasma phase, and the plasma current shown in Fig. 5 is directly related to it. At last, we noted an instability on both the current and potential showing in the work of Alam et al., as highlighted in plate d. In principle, such instability can arise from the instability of the external circuit or from the plasma chemistry. Preliminary, there are indication supporting the chemical instability due to the presence of three autocatalytic reactions in the set of elementary reactions involved in the plasma-chemistry mechanism of water splitting. They are the reaction 6, 7 and 8 in Tab. 3. They are called reactions of autocatalysis because one plasma free electron creates other two after the collision of water with one plasma free electron. Those autocatalytic reaction allows for oscillatory variation on the plasma electron density, which can be associated with the current oscillations seen in plate d.

III.c) Spectrum and quantity of radicals formed in humidified noble-gas plasma

As seen above, the PFOA degradation induced by hydrate electron within the so-called Electrified Plasma Liquid Interface (EPLI) alone cannot justify the energetic performance observed by the experiments of Stratton et al. and Alam et al. For this reason, in this section, we analyse the spectrum of radicals formed during a discharge in the noble gas phase containing water vapor, searching for a potential key radical that could explain the performance observed by Stratton et al.

Recently, Sankaran team [31] identified that the equilibrium vapor pressure of water in the EPLI introduces water vapor in the plasma phase, so that noble-gas jet plasma serves as a weakly ionized gas to split water vapor via the free-electron impact. By solving the Boltzmann equation (BE) [6] considering both weakly ionized gases and a uniform electric field, the authors found eight elementary reactions involved in the plasma-chemistry mechanism of water splitting, and that is shown in Tab. 3. Those reactions have the largest rate constants (or electron rate coefficients). The balanced reaction resulted from the adding of eight electron-impact water splitting reactions from Tab. 3 is shown below.

	Elementary reaction
1.	$e^- + H_2O \rightarrow H^\bullet + OH^-$
2.	$e^- + H_2O \rightarrow 2H^\bullet + O^-$
3.	$e^- + H_2O \rightarrow H^- + OH^\bullet$
4.	$e^- + H_2O \rightarrow e^- + H^\bullet + OH^\bullet$
5.	$e^- + H_2O \rightarrow e^- + 2H^\bullet + O^\bullet$
6.	$e^- + H_2O \rightarrow 2e^- + H^+ + OH^\bullet$
7.	$e^- + H_2O \rightarrow 2e^- + H^\bullet + OH^+$
8.	$e^- + H_2O \rightarrow 2e^- + 2H^\bullet + O^+$

Table 3: Set of reactions for the electro impact water splitting obtained by Toth et al. [31]

In plasma phase, the water molecule splits into two major classes of fragments, the radical fragment set {●H, ●OH and ●O} and the ionic fragment set {O^-, O^+, OH^-, OH^+, H^-, H^+}. These two classes of fragments receive different treatments in this work because only the radicals have value for pollutant degradation. Among the radical fragments in Eq. (19), the H radical is formed in large amounts—three times the quantity of the OH radical and nine times that of the O radical. Quantitatively, the H radical is the principal radical responsible for degrading the pollutant at the gas/liquid interface.

$$8\,H_2O_{gas} \rightarrow 9\,H^\bullet{}_{gas} + 3\,OH^\bullet{}_{gas} + O^\bullet{}_{gas} + O^-{}_{gas} + O^+{}_{gas} + OH^-{}_{gas} + OH^+{}_{gas} + H^-{}_{gas} + H^+{}_{gas} \quad (19)$$

Tab. 4 informs the density of radical in humidified noble gas phase. Using two techniques of ultra-violet absorption spectroscopy, Schroter et al.[32] measured absolute densities of O (#O) and OH (#OH), whose relative ratio #OH/#O approaches value of 10 at maximum value of water saturation in the noble gas. Instead, our analysis of relative ratio #OH/#O reads 3. The mismatches of one order of magnitude informs our theoretical analysis is incomplete. The reaction 19 only takes the electron impact of H_2O as source of radicals. A fine tune can be made by addicting contribution of other plasma processes like dissociative excitation transfer from metastable

Ar atoms and Ar dimer excimers proposed by Luo et al. [33] Tab. 4 also allows for comparison between models. The density of OH was measured to be two orders of magnitude smaller than that of H for the model of Luo et al., [33] meaning a mismatch of one order of magnitude with our analysis based on the reaction 19. The incompletion on the model of Luo et al. lies on the fact that only one electro-impact dissociation reaction of H_2O was considered. Instead, this work used eight electro-impact dissociation reaction of H_2O found in the work of Toth et al. [6] to propose the reaction 19.

Furthermore, a second and fundamental argument is shown below, supporting the thesis that the H radical is the primary species promoting PFAS degradation at the gas-liquid interface. The wall sticking coefficients (γ) for both the H radical and the O radical are below 0.05, whereas several other noble gas fragments along with the OH radical have values of 1.00 [32]. This means that when γ equals 1, virtually all collisions between similar fragments result in a chemical bond, whereas only a proportionately smaller number of collisions lead to the formation of a new chemical compound when γ approaches zero. Consequently, neither the H radical nor the O radical will tend to recombine to form H_2 and O_2, respectively. Instead, both radicals will tend to form bonds with any heavier fragments available in large amounts within the system, such as stable molecules. It is very well known that discharge in O_2 gas produces ozone (O_3), with O_2 being the stable molecule in large amounts that reacts with the O radical to form O_3 [27]. In the case of the H radical, it is likely that the it reacts with stable H-containing molecules, extracting an H fragment in a process known in catalysis as H-subtraction. A recently published paper is recommended for revisiting in great detail the interpretation of plasma-induced H-subtraction [34].

Finally, a third foundational argument endorses the thesis of H radical is the key radical in PFOAS degradation. This concerns the lifetime of the species, or the relaxation time, which measures how long time it takes for a specie to be reduced to a minimum concentration. As previously mentioned, the radical H and radical O have γ ≤ 0.05, which significantly distinguishes them from other radicals like OH and noble gas fragments, which have γ ~ 1.00. Of the radicals formed in reaction 19, only the OH radical recombines rapidly, such that only the stable product H_2O_2 is observed dissolved in the water used to scrub the plasma effluent,[2] (see Fig. 2 depicting this phenomenon). The recombination of the OH radical, producing H_2O_2, primarily occurs within the plasma volume, making the gas-phase OH radical short-lived in this context. In contrast, both the H and O radicals are long-lived in noble gas due to two fundamental reasons: (a) their recombination takes longer relaxation time, and (b) no stable product can result from their collision with any noble gas fragment.

III.d) CRN–4 analysis for the gas/liquid interface formed with the plasma effluent

Given all arguments above, Fig. 6 shows the CRN–4 that is the proposed mechanism for PFOA/PFOS degradation in the electrochemical configuration employed by Stratton et al./Alam et al. CRN–4 develops in the gas/liquid interface, which is formed when the plasma effluent is directly pumped into the water matrix. In this CRN–4, the plasma-induced gas-phase H radical readily react out with PFOA and water through reaction 20 and 21 respectively

$$H^{\bullet}_{gas} + C_8HF_{15}O_{2_{liq}} \xrightarrow{k18} radical^{\bullet}_{liq} + \mathrm{HF}_{liq} \quad (20)$$

$$H^{\bullet}_{gas} + H_2O_{liq} \xrightarrow{k19} H_{2_{gas}} + \mathrm{OH}^{-}{}_{liq} \quad (21)$$

Electrical properties of the plasma	#O	#H	#OH	$\frac{\#OH}{\#O}$	$\frac{\#OH}{\#H}$	Ref.
Radio-frequency Pulsed jet discharge in He	3×10^{13}	–	3×10^{14}	10.00	–	[32]
Nanosecond Pulsed filamentary discharge in H_2O-Ar	–	–	–	–	0.01	[33]
N/A	$1x$	$9x$	$3x$	3.00	0.33	Reaction 19, This work

Table 4: Experimental and theoretical density of radicals in humidified noble gas plasma

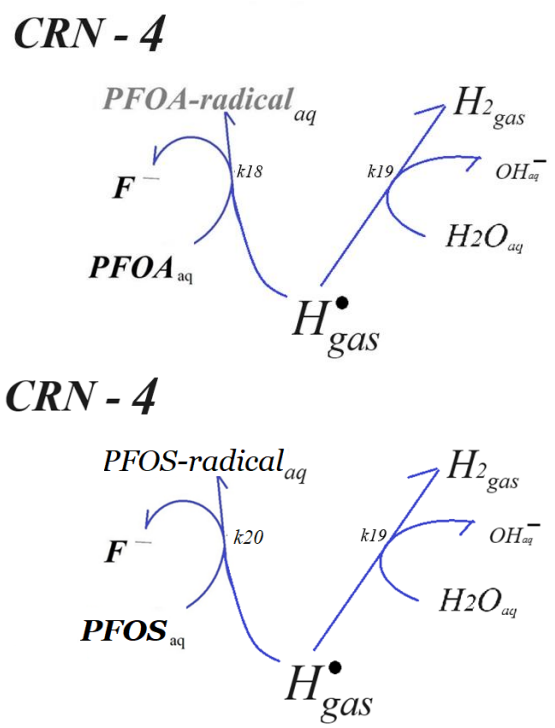

Figure 6. Chemical Reaction Network (CNR-4) to explain the results of both Stratton et al.[8] on top and Alam et al.[21] on bottom, which includes the plasma effluent H-radical reaction with the pollutant in the gas/liquid interface. Water is the composition of the liquid phase, reason for using subscription aq.

The long-living gas-phase H radical concentration in the plasma effluent evolves according Eq. 22, and the bulk concentration of PFOA evolves according Eq. 23

$$\frac{d[\mathrm{H}^{\bullet}_{gas}]}{dt} = -S\{k_{18}[\mathrm{H}^{\bullet}_{gas}]\,\Gamma_{PFOA} + k_{19}[\mathrm{H}^{\bullet}_{gas}]\} \quad (22)$$

$$\frac{d[PFOA]_b}{dt} = -S\{k_{18}[\mathrm{H}^{\bullet}_{gas}]\,\Gamma_{PFOA}\} \quad (23)$$

where k_{18} and k_{19} stand for the rate constant of reaction 20 and 21, respectively; S stands for the total area of the interface gas/liquid, and Γ_{PFOA} means the surface excess of PFOA in the gas/liquid interface of the bubble. The initial values of H-radical concentration in the plasma effluent, $[\mathrm{H}^{\bullet}_{gas}]_0$, and the initial pollutant concentration in the liquid phase, either $[\mathrm{PFOA}]_0$ and $[\mathrm{PFOS}]_0$, must be informed in order to implement the algorithm to solve the set of Eqs. 22 and 23 with numerical methods. Tab. 5 informs the values to be attributed to those and other parameters. The surface excess of PFOA is computed by Eq. 24

$$\Gamma_{PFOA} = \Gamma^{Max}_{PFOA}\,\frac{[PFOA]_b}{[PFOA]_b + b} \quad (24)$$

where Γ^{Max}_{PFOA} and b are constants standing for PFOA's maximum surface excess and surface activity, respectively. In Eq. 24, $[PFOA]_b$ means the bulk concentration of PFOA. According to Costanza et al.[26], $\Gamma^{Max}_{PFOA} = 0{,}38\ mg\ m^{-2}$ (91.18 10^{-3} mol m^{-2}) and $b = 14{,}7\ mg\ L^{-1}$ (35.5 μM).

Eqs. 22 and 23 form the dynamical system for PFOA degradation driven by gas-phase H radical and whose set of parameters is described in Tab. 5. For solving numerically this system, values must be attribute to five parameters, $[\mathrm{H}^{\bullet}_{gas}]_0$, $[\mathrm{PFOA}]_0$, S, k_{18} and k_{19}. According to reaction 17, the initial gas concentration of hydrogen Radical could be attemptedly attributed to the value of tree times the concentration of plasma radical OH, being the latter measured by Schröter et al. [35] In principle, values of k_{18} and k_{19} can be estimated by adjusting the dynamical system, defined by the differential Eqs. 22 and 23, to the value of t_{90}, following similar approached used before. [36]

The recent work of Alam et al. [21] supports the mechanistic proposal of CNR-4. The authors developed an effective method to transport the PFOS dissolved in a 58 cm tall column of water up to the surface based on principles of colloid science. Given its long apolar carbon chair and polar head, the aqueous PFOS molecule exhibits surfactant properties, such as adsorbing on the gas/liquid interface, which results in an elevated concentration of PFOS on the bubble interface in comparison to the bulk liquid. By creating small Argon bubbles of 0.6 to 0.8 mm diameter at the reactor bottom, Alam et al demonstrate that the PFOS concentration on the top surface increases two time relative to the average, whereas the PFOS concentration on the bottom aqueous layer on the reactor decreases by one third. In addition to this significant increase in the local PFOS concentration on the top surface, the reactor of Alam et al. holds the plasma effluent strictly at the reactor headspace, which contrast with the experiments of Straton et al. that reinjects the plasma effluent in the water matrix. Yet, reactor of Alam et al. hits similar energy efficiency, which reinforces the on top gas/liquid interface as being the active interface for CNR-4.

Lastly, CNR-4, as described by the Eqs. 22 and 23 (with Eq. 24 depending on them) is quite general. It does not take into account the specifics of the reactor, particularly the gas/liquid interface. In the experiments conducted by Alam et al., the parameter S in Eqs. 22 and 23 is well defined because the diameter of the top layer is 25 cm and the reactor does not produce foam. Therefore, in principle, there is possibility of applying CNR-4.

Parameters	Values	Unit	Ref.	meaning
k_{18}	n/a	L mol^{-1} s^{-1}		Rate constant of reaction 18
k_{19}	n/a	L mol^{-1} s^{-1}		Rate constant of reaction 19
Γ_{PFOA}^{Max}	91.18 10^{-3}	mol m^{-2}	[26]	PFOA's maximum surface excess
b	35.5	μM	[26]	PFOA's maximum surface activity
$[H^{\bullet}_{gas}]_0$	$3[OH^{\bullet}_{gas}]$		This work	Initial gas concentration of hydrogen Radical
$[OH^{\bullet}_{gas}]$	0.49×10^{-9}	mol cm^{-3}	[35]	Initial gas concentration of hydrogen OH
S	n/a	cm		total area of the interface gas/liquid
$[PFOA]_0$	2.0×10^{-5}	mol L^{-1}	[8]	Initial bulk aqueous concentration of PFOA
$[PFOS]_0$	2.7×10^{-7}	mol L^{-1}	[21]	Initial bulk aqueous concentration of PFOS

Table 5: Parameters of the CRN-4.

IV. Conclusion

This work presents a theoretical analysis to decipher the nature of radicals allowing for the outstanding energetic performance of PFAS degradation observed for the electrochemical configuration of cold plasma in the work of Stratton et al. For that, this work presented a chemical dynamical model to explain the formation and reactivity of both hydrated electrons (e^-_{aq}) and radical-H in the electrified plasma/liquid interface (EPLI). Besides, a second interface demonstrated importance for PFAS degradation, the gas/liquid interface. For this reason, the gas phase radicals that are induced by a plasma in presence of water vapor is thoroughly studied aiming to elect a gas-phase radical that is crucial for PFAS degradation.

In general, EPLI-induced e^-_{aq} promotes PFOA (model CRN-1) and PFOS (model CRN-2) degradation with poor faradaic efficiency (< 0.01%), meaning that over 70% of the EPLI-induced e^-_{aq} promotes water splitting, thus co-producing gaseous hydrogen. Such low faradaic efficiency is intrinsically associated to the low PFOA concentration. When the energy performance of EPLI-based experiments is confronted, PFOA degradation displays one thousand higher energy performance for bench experiments in comparison to our empirical theoretical analysis, which is a clear indication that EPLI-induced e^-_{aq} is not acting alone in the bench experiments. A second important radical in the electrified plasma/liquid interface was then analysed, the EPLI-induced radical H. However, the energy performance only improved slightly when considering the in-situ H-radical (model CRN-3).

Finally, we analyse the spectrum of radicals formed in the plasma phase that could possibly be playing roles in the gas/liquid interface. Very presumably, in bench experiments, plasma-phase radical H is being generated by plasma interaction with either co-produced hydrogen or water vapor, and both sources of radical H are causing the extra PFOA abatement, thus better energy performance in comparison to our CRN-1 analysis.

In view of all data disclosed above, we conclude that (a) there is none strategy to increase the faradaic efficiency in the electrified plasma/liquid interface toward PFOA degradation by e^-_{aq} because it is intrinsically related to the low PFOA concentration in water bodies; besides, the production of gaseous hydrogen holds the major share on the faradaic efficiency of e^-_{aq} ; and, (b) the gas phase plasma-induced H radical is a long lived specie with potential for degrading PFOA mostly at the ordinary gas/liquid interface. The recent work of Alam et al. supports our concluding hypothesis (CRN-4) that ordinary gas/liquid interface is the key local reactor responsible for the energetic outperformance of PFOA degradation by plasma water treatments

V. Acknowledgment

I gratefully acknowledge direct support of the National Council for Scientific and Technological Development (CNPq, 102191/2024-7) and the indirect support of RCGI – Research Centre for Greenhouse Gas Innovation, hosted by the University of São Paulo (USP) and sponsored by FAPESP – São Paulo Research Foundation (2014/50279-4 and 2020/15230-5) and Shell Brazil.

VI. References

[1] P. Rumbach, D.M. Bartels, R.M. Sankaran, D.B. Go, "The solvation of electrons by an atmospheric-pressure plasma," *Nature Commun.*, vol. 6, 2015, 7248.

[2] P. Rumbach, M. Witzke, R.M. Sankaran, D.B. Go, "Decoupling Interfacial Reactions between Plasmas and Liquids: Charge Transfer vs Plasma Neutral Reactions," *J. Am. Chem. Soc.*, vol. 135, no. 44, 2013, pp. 16264-16267.

[3] M. Sahni, B.R. Locke, "Quantification of Hydroxyl Radicals Produced in Aqueous Phase Pulsed Electrical Discharge Reactors," *Ind. Eng. Chem. Res.*, vol. 45, no. 17, 2006, pp. 5819-5825.

[4] R.L. Bruce, S. Kai-Yuan, "Review of the methods to form hydrogen peroxide in electrical discharge plasma with liquid water," *Plasma Sources Sci. Technol.*, vol. 20, no. 3, 2011, 034006.

[5] R. Burlica, K.Y. Shih, B.R. Locke, "Formation of H2 and H2O2 in a Water-Spray Gliding Arc Nonthermal Plasma Reactor," *Ind. Eng. Chem. Res.*, vol. 49, no. 14, 2010, pp. 6342-6349.

[6] J.R. Toth, R. Hawtof, D. Matthiesen, J.N. Renner, R.M. Sankaran, "On the Non-Faradaic Hydrogen Gas Evolution from Electrolytic Reactions at the Interface of a Cathodic Atmospheric-Pressure Microplasma and Liquid Water Surface," *J. Electrochem. Soc.*, vol. 167, no. 11, 2020, 116504.

[7] R.K. Singh, N. Multari, C. Nau-Hix, R.H. Anderson, S.D. Richardson, et al., "Rapid Removal of Poly- and Perfluorinated Compounds from Investigation-Derived Waste (IDW) in a Pilot-Scale Plasma Reactor," *Environ. Sci. Technol.*, vol. 53, no. 19, 2019, pp. 11375-11382.

[8] G.R. Stratton, F. Dai, C.L. Bellona, T.M. Holsen, E.R. Dickenson, S.M. Thagard, "Plasma-Based Water Treatment: Efficient Transformation of Perfluoroalkyl Substances in Prepared Solutions and Contaminated Groundwater," *Environ. Sci. Technol.*, vol. 51, no. 3, 2017, pp. 1643-1648.

[9] R.K. Singh, S. Fernando, S.F. Baygi, N. Multari, S.M. Thagard, et al., "Breakdown Products from Perfluorinated Alkyl Substances (PFAS) Degradation in a Plasma-Based Water Treatment Process," *Environ. Sci. Technol.*, vol. 53, no. 5, 2019, pp. 2731-2738.

[10] C. Nau-Hix, N. Multari, R.K. Singh, S. Richardson, P. Kulkarni, R.H. et al., "Field Demonstration of a Pilot-Scale Plasma Reactor for the Rapid Removal of Poly- and Perfluoroalkyl Substances in Groundwater," *ACS ES&T Water*, vol. 1, no. 3, 2021, pp. 680-687.

[11] S. Biswas, S. Yamijala, B.M. Wong, "Degradation of Per- and Polyfluoroalkyl Substances with Hydrated Electrons: A New Mechanism from First-Principles Calculations," *Environ. Sci. Technol.*, vol. 56, no. 12, 2022, pp. 8167-8175.

[12] W.A. Maza, V.M. Breslin, J.C. Owrutsky, B.B. Pate, A. Epshteyn, "Nanosecond Transient Absorption of Hydrated Electrons and Reduction of Linear Perfluoroalkyl Acids and Sulfonates," *Environ. Sci. Technol. Lett.*, vol. 8, no. 7, 2021, pp. 525-530.

[13] R. Akolkar, R.M. Sankaran, "Charge transfer processes at the interface between plasmas and liquids," *J. Vac. Sci. Technol. A*, vol. 31, no. 5, 2013, 050811.

[14] A. Mota-Lima, "The Electrified Plasma/Liquid Interface as a Platform for Highly Efficient CO2 Electroreduction to Oxalate," *J. Phys. Chem. C*, vol. 124, no. 20, 2020, pp. 10907-10915.

[15] D.J. Burns, P. Stevenson, P.J.C. Murphy, "PFAS removal from groundwaters using Surface-Active Foam Fractionation," *Remediation J.*, vol. 31, no. 4, 2021, pp. 19-33.

[16] D.C. Johnson, V.A. Shamamian, J.H. Callahan, F.S. Denes, S.O. Manolache, et al., "Treatment of Methyl tert-Butyl Ether Contaminated Water Using a Dense Medium Plasma Reactor: A Mechanistic and Kinetic Investigation," *Environ. Sci. Technol.*, vol. 37, no. 20, 2003, pp. 4804-4810.

[17] R. Aerts, X. Tu, W. Van Gaens, J.C. Whitehead, A. Bogaerts, "Gas Purification by Nonthermal Plasma: A Case Study of Ethylene," *Environ. Sci. Technol.*, vol. 47, no. 12, 2013, pp. 6478-6485.

[18] M.B. Chang, S.J. Yu, "An Atmospheric-Pressure Plasma Process for C2F6 Removal," *Environ. Sci. Technol.*, vol. 35, no. 8, 2001, pp. 1587-1592.

[19] M.J. Johnson, W.A. Maza, V.M. Breslin, D.R. Boris, T.B. Petrova, et al., "Low power degradation of perfluorooctane sulfonate (PFOS) in water

using a nanosecond pulsed atmospheric pressure plasma," *Plasma Sources Sci. Technol.*, vol. 31, no. 8, 2022.

[20] R. Hayashi, H. Obo, N. Takeuchi, K. Yasuoka, "Decomposition of Perfluorinated Compounds in Water by DC Plasma within Oxygen Bubbles," *Electr. Eng. Jpn.*, vol. 190, no. 3, 2015, pp. 9-16.

[21] D. Alam, S. Lee, J. Hong, D.F. Fletcher, X. Liu, et al., "Influence of bubble size on perfluorooctanesulfonic acid degradation in a pilot scale non-thermal plasma treatment reactor," *Chem. Eng. J.*, vol. 489, 2024.

[22] D. Alam, S. Lee, J. Hong, D.F. Fletcher, D. McClure, et al., "Experimental investigations of Per- and Poly-fluoroalkyl substances (PFAS) degradation by non-thermal plasma in aqueous solutions," *J. Environ. Chem. Eng.*, vol. 11, no. 6, 2023.

[23] G.V. Buxton, C.L. Greenstock, W.P. Helman, A.B. Ross, "Critical Review of rate constants for reactions of hydrated electrons, hydrogen atoms and hydroxyl radicals (·OH/·O− in Aqueous Solution," *J. Phys. Chem. Ref. Data*, vol. 17, no. 2, 1988, pp. 513-886.

[24] A. Mota-Lima, J.F. do Nascimento, O. Chiavone-Filho, C.A.O. Nascimento, "Electrosynthesis via Plasma Electrochemistry: Generalist Dynamical Model To Explain Hydrogen Production Induced by a Discharge over Water," *J. Phys. Chem. C*, vol. 123, no. 36, 2019, pp. 21896-21912.

[25] I. Gonçalves, J. Barauna, F. Cunha-Filho, O. Chiavone-Filho, J. Vitoriano, et al., "Reduction of Aqueous Ag+ Steered by Electrochemical Plasma: Connecting the Bulk pH Variation with the Reaction Pathways for Hydrated Electrons," *J. Braz. Chem. Soc.*, 2019.

[26] J. Costanza, M. Arshadi, L.M. Abriola, K.D. Pennell, "Accumulation of PFOA and PFOS at the Air--Water Interface," *Environ. Sci. Technol. Lett.*, vol. 6, no. 8, 2019, pp. 487-491.

[27] B. Eliasson, M. Hirth, U. Kogelschatz, "Ozone synthesis from oxygen in dielectric barrier discharges," *J. Phys. D: Appl. Phys.*, vol. 20, no. 11, 1987, 1421.

[28] R.A. Davies, A. Hickling, "686. Glow-discharge electrolysis. Part I. The anodic formation of hydrogen peroxide in inert electrolytes," *J. Chem. Soc.*, 1952, pp. 3595-3602.

[29] J. Liu, B. He, Q. Chen, J. Li, Q. Xiong, et al., "Direct synthesis of hydrogen peroxide from plasma-water interactions," *Sci. Rep.*, vol. 6, 2016, 38454.

[30] D.C. Martin, D.T. Elg, H.E. Delgado, H.M. Nguyen, P. Rumbach, et al., "Optical and Chemical Measurements of Solvated Electrons Produced in Plasma Electrolysis with a Water Cathode," *Langmuir*, vol. 40, no. 28, 2024, pp. 14224-14232.

[31] G.J.M. Hagelaar, L.C. Pitchford, "Solving the Boltzmann equation to obtain electron transport coefficients and rate coefficients for fluid models," *Plasma Sources Sci. Technol.*, vol. 14, no. 4, 2005, 722.

[32] S. Schroter, A. Wijaikhum, A.R. Gibson, A. West, H.L. Davies, et al., "Chemical kinetics in an atmospheric pressure helium plasma containing humidity," *Phys. Chem. Chem. Phys.*, vol. 20, no. 37, 2018, pp. 24263-24286.

[33] Y. Luo, A.M. Lietz, S. Yatom, M.J. Kushner, P.J. Bruggeman, "Plasma kinetics in a nanosecond pulsed filamentary discharge sustained in Ar--H2O and H2O," *J. Phys. D: Appl. Phys.*, vol. 52, no. 4, 2019.

[34] N. Lim, Y. Wu, M.J. Gordon, "Impact of Pressure and Hydrogen Dilution on the Kinetics of Methane Decomposition in AC-Excited, High Pressure Plasmas," *Plasma Chem. Plasma Process.*, vol. 44, no. 1, 2023, pp. 47-64.

[35] S. Schröter, A. Wijaikhum, A.R. Gibson, A. West, H.L. Davies, et al., "Chemical kinetics in an atmospheric pressure helium plasma containing humidity," *Phys. Chem. Chem. Phys.*, vol. 20, no. 37, 2018, pp. 24263-24286.

[36] A. Mota-Lima, "Ratio Oxalate to Formate Tuned by pH During CO2 Reduction Driven by Solvated Electron at the Electrified Plasma/Liquid Interface," *Electrocatalysis*, vol. 11, no. 6, 2020, pp. 618-627.

Supplementary Material is available from the author upon request.

